Geophysical Prospecting 31, 608–626, 1983.

AUTOMATIC THREE-LAYER, THREE-DIMENSIONAL DECONVOLUTION OF THE PAYS DE BRAY ANTICLINE*

E. ALESSANDRELLO, M. BICHARA and J. LAKSHMANAN**

ABSTRACT

ALESSANDRELLO, E., BICHARA, M. and LAKSHMANAN, J. 1983, Automatic Three-Layer, Three-Dimensional Deconvolution of the Pays de Bray Anticline, Geophysical Prospecting 31, 608–626.

Gravity data have been transformed into a three-layer, three-dimensional model by using an automatic procedure based on linear filtering. The Bouguer anomaly is first transformed by linear filtering into density variations located between two planes 1100 and 2500 m deep. These densities are then transformed into thicknesses with a constant density contrast of 0.4 g/cm^3 with two geological constraints for the second and third interface:

—minimum at 2500 m depth;
—maximum below a variable limit given by geology.

This gives the contact between the second and third layer. Differences between measured and computed gravity are then applied by a similar procedure to a layer located between depths of 0 and 500 m, giving the contact between the first and second layer. Interesting secondary anticlines and transverse faults are shown by various structural maps.

RESUME

ALESSANDRELLO, E., BICHARA, M. et LAKSHMANAN, J. 1983, Déconvolution Gravimétrique Tridimensionnelle et à Trois Couches de l'Anticlinal du Pays de Bray, Geophysical Prospecting 31, 608–626.

Utilisant un procédé automatique de déconvolution basé sur un filtrage linéaire, les auteurs ont transformé des données gravimétriques existantes en un modèle tridimensionnel à trois couches. L'anomalie de Bouguer est d'abord transformée par filtrage linéaire, en variations de densité d'une plaque horizontale, située entre 1100 et 2500 m de profondeur. Ces

* Paper read at the 43rd meeting of the European Association of Exploration Geophysicists, Venice, May 1981, revised version accepted December 1982.
** Compagnie de Prospection Géophysique Française, 77–79 avenue Victor Hugo, 92500 Rueil-Malmaison, France.

 0016–8025/83/0800–0608 $02.00

densités sont ensuite transformées en épaisseurs en utilisant un contraste constant de densité de 0.4 g/cm^3, avec deux contraintes géologiques pour la limite entre la deuxième et la troisième couche:

—minimum fixe à 2500 m de profondeur;
—maximum situé sous une limite variable en chaque point, fixée d'après la géologie.

Ayant obtenu ainsi le contact entre la deuxième et la troisième couche, la différence entre le champ mesuré et le champ dû à cette première structure est appliquée à une deuxième plaque située entre 0 at 500 m de profondeur, pour en déduire le contact entre la première et la deuxième couche. Les diverses cartes structurales obtenues mettent en évidence plusieurs anticlinaux secondaires, ainsi que de nombreuses failles transverses.

1. Introduction

The hydrogeology department of CPGF has been charged by the French Ministry of Agriculture (DDA of Seine Maritime) to evaluate ground water resources in the Pays de Bray area, northwest of Paris. In order to supply detailed structural information from the area, it was decided to carry out a quantitative analysis of existing gravity data, published by the BRGM, at a scale of 1 : 200 000.

The computer program developed by Lakshmanan (1973) and Bichara and Lakshmanan (1979) supplies, after introducing various geological constraints, a three-layer, three-dimensional model. The procedure, using linear filtering, is much faster than an iterative system described by La Porte (1963), involving a two layer method.

The procedure works as follows:

—in the first step, construction of density maps of thick horizontal plates by linear filtering;
—the use of geological buffers in the construction of the model.

2. Existing Data

We used the BRGM gravity maps of France, i.e., sheets of Abbeville, Rouen, Amiens, and Paris, corresponding to the southeast half of the famous Pays de Bray anticline (between Neufchatel-en-Bray and Beauvais), and starting with the Bouguer anomaly with a 2.3 g/cm^3 density. Unfortunately, the station spacing is quite high: 5–10 km^2 per station, equivalent to a 2.5–3 km square grid, and the measurements are rather old (BRGM North American gravity meter). The maps were digitized on a 2 × 2 km square grid. The interpretation was made on 20 × 20 = 400 central points, using a maximum of 28 × 28 = 784 points. Location of the area is shown in fig. 1.

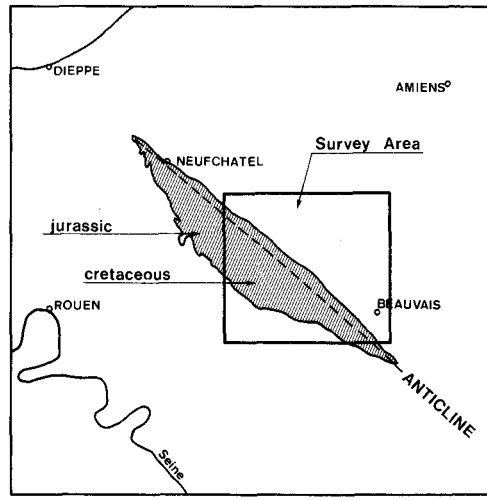

Fig. 1. Location of the survey. [Situation de l'étude.]

The Bouguer anomaly corresponding to the 400 central points is shown in fig. 2. The values increase from −30 mGal in the southwest towards the anticline, along which −15 mGal is observed towards the southeast and −4 towards the northwest. Northeast of the main anticline, the Bouguer anomaly stays high (−4 to −10), decreases along a syncline (−16 to −20), and finally increases to −13 in the northeast corner.

The maximum Bouguer variation is thus 26 mGal, the average anomaly compared to the minimum is 17 mGal, and the median anomaly is 22.7 mGal.

3. Systematic Deconvolution by Variable Density Horizontal Sheets

For each sheet, the entire Bouguer anomaly is used, giving four different density maps. The following depths were selected, starting from a datum plane located at 100 m above sea level:

0–500 m
500–1500 m
1500–2500 m
2500–3500 m

For each density map, the corresponding gravity field is computed as well as a map of differences between measured and computed fields and a map of the correlation coefficient r_0. This coefficient corresponds to the correlation between the computed field and measured Bouguer anomaly, inside a $7h \times 7h$ moving window, where h is the central depth of the plate:

$$r_0 = \frac{\sum_{\Delta 1 \times \Delta 2} (Th_i - Th_0)(\mathrm{Exp}_i - \mathrm{Exp}_0)}{\sqrt{[\sum_{\Delta 1 \times \Delta 2} (Th_i - Th_0)^2 (\mathrm{Exp}_i - \mathrm{Exp}_0)^2]}},$$

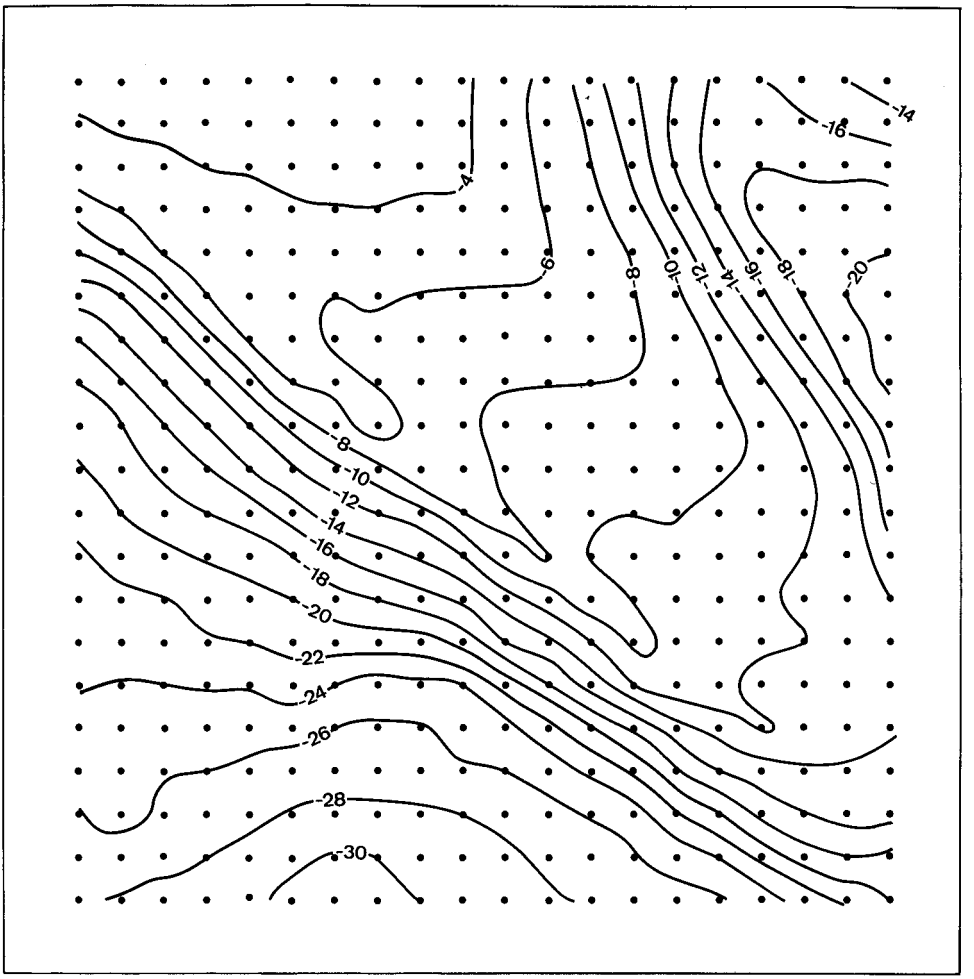

Fig. 2. Bouguer anomaly (in mGal). [Anomalie de Bouguer (mGal).]

where Th_i is the computed value at the running point i, Th_0 is the computed value at the considered point 0, Exp_i is the experimental Bouguer value at the running point i, Exp_0 is the experimental Bouguer value at the considered point 0, and $\Delta 1$, $\Delta 2$ are the intervals defining the moving window.

It should be noted that the use of a correlation coefficient, or rather of a similarity coefficient for depth determination, has been suggested by Naudy (1971). However, the following two points are different:

—Naudy's method supposes several standard shapes for the anomaly, while we determine the shape itself by deconvolution.

—Naudy supposes a two-dimensional anomaly and only examines profiles, while we study three-dimensional anomalies.

Figures 3 to 6 show the four computed density maps. The general statistics are as follows:

Bouguer anomaly

maximum	−2.3 mGal;
median	−8.2 mGal;
minimum	−30.9 mGal;
variation of amplitude	28.6 mGal;
median variation	M = 22.7 mGal.

In order to give a homogeneous set of densities corresponding to a 1000-m-thick slab, the 0- to 500-m map was transformed into a 0- to 1000-m map.

In fig. 7, variations of mean square difference of the whole area are shown as functions of the average depth of each slab. It can be seen that the mean square difference increases with depth without a minimum. However, this parameter increases quite suddenly after an average depth of about 2000 m (*see* table 1).

The correlation coefficient is very close to 1. The obtained values decrease for depths greater than 2000 m for the entire area, 1700 m for the main anticline (i.e., 1200 m for its top), and 2200 m for a syncline located 8 km SW of the center of the

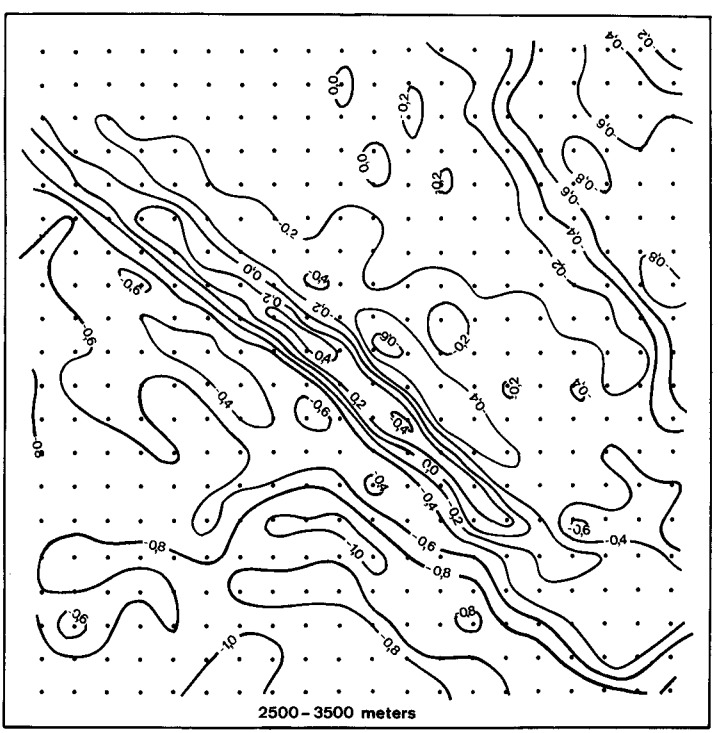

Fig. 3. Inverted density between 2500 and 3500 m (g/cm^3). [Densité obtenue par inversion, entre 2500 et 3500 m (g/cm^3).]

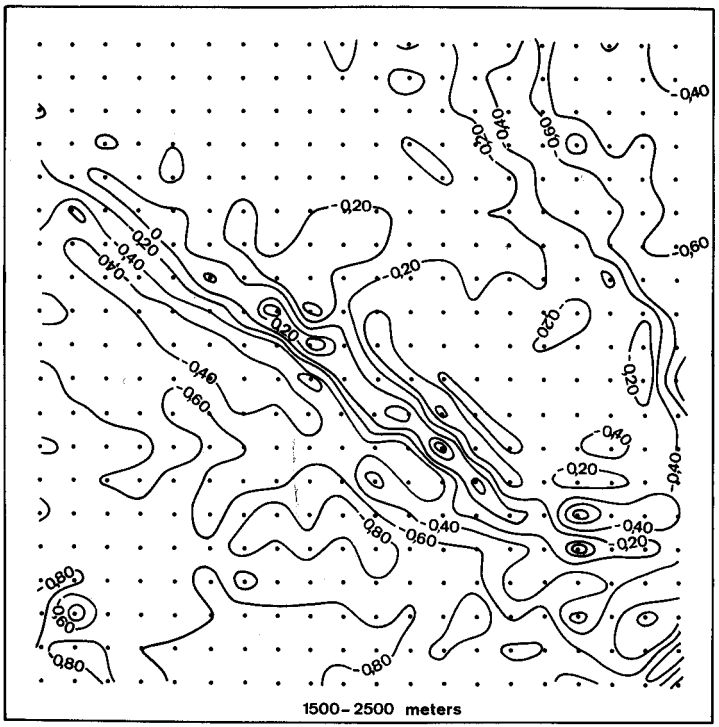

Fig. 4. Inverted density between 1500 and 2500 m (g/cm^3). [Densité obtenue par inversion entre 1500 et 2500 m (g/cm^3).]

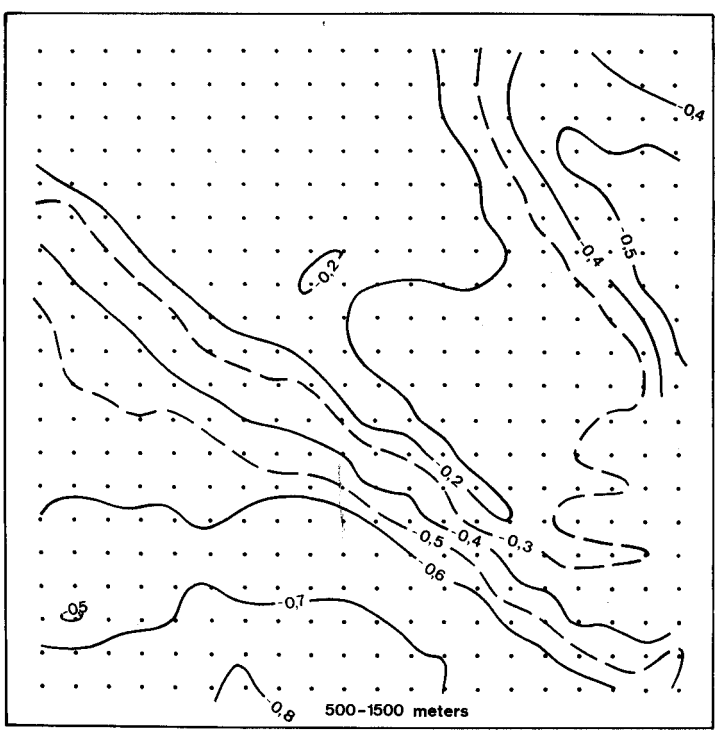

Fig. 5. Inverted density between 500 and 1500 m (g/cm^3). [Densité obtenue par inversion entre 500 et 1500 m (g/cm^3).]

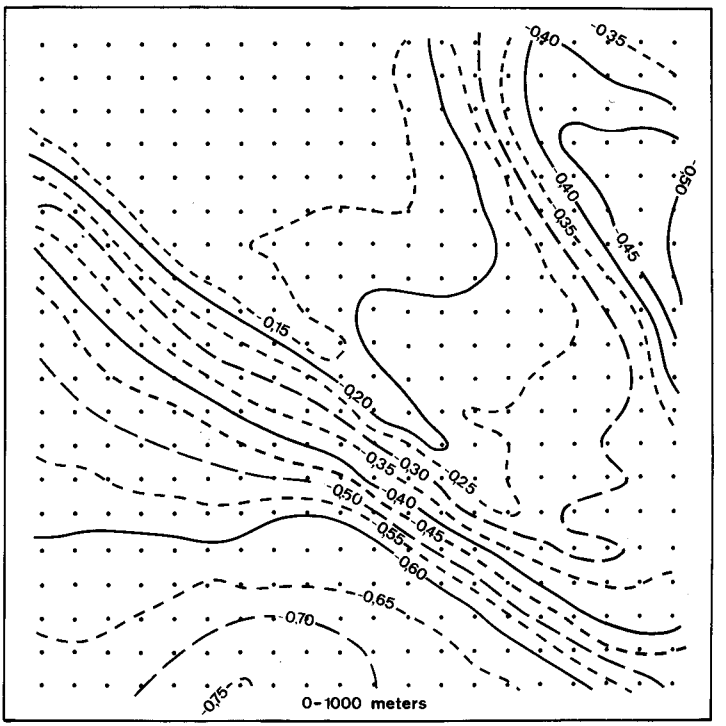

Fig. 6. Inverted density between 0 and 1000 m (g/cm^3). [Densité obtenue par inversion entre 0 et 1000 m (g/cm^3).]

main anticline. It should be pointed out that the actual depths to the top of the anticline found in five wells were 1110, 1207, 1078, 959 and 979 m (datum plane 100 m above sea level).

It should be noted that, if both mean square difference and correlation coefficient show a semi-horizontal section for the plate center located between 1000 and 2000 m, another improvement in these criteria can be seen when the plate outcrops.

Table 1. *Correlation statistics and average densities.*

Depth (m)	Mean square difference		Correlation coefficient		Relative densities (g/cm^3)		
	mGal	Percent of M	Whole area	Main anticline	Maximum	Minimum	Amplitude of variation
0–500	0.05	0.2	0.99999	0.99999	−0.11	−1.51	1.40
(0–1000)	—	—	—	—	(−0.06)	(−0.76)	(0.70)
500–1500	0.15	0.7	0.99988	0.99993	−0.016	−0.814	0.80
1500–2500	0.21	0.9	0.99964	0.99983	+0.53	−0.94	1.47
2500–3500	0.46	2.0	0.99772	0.99859	+0.57	−1.12	1.69

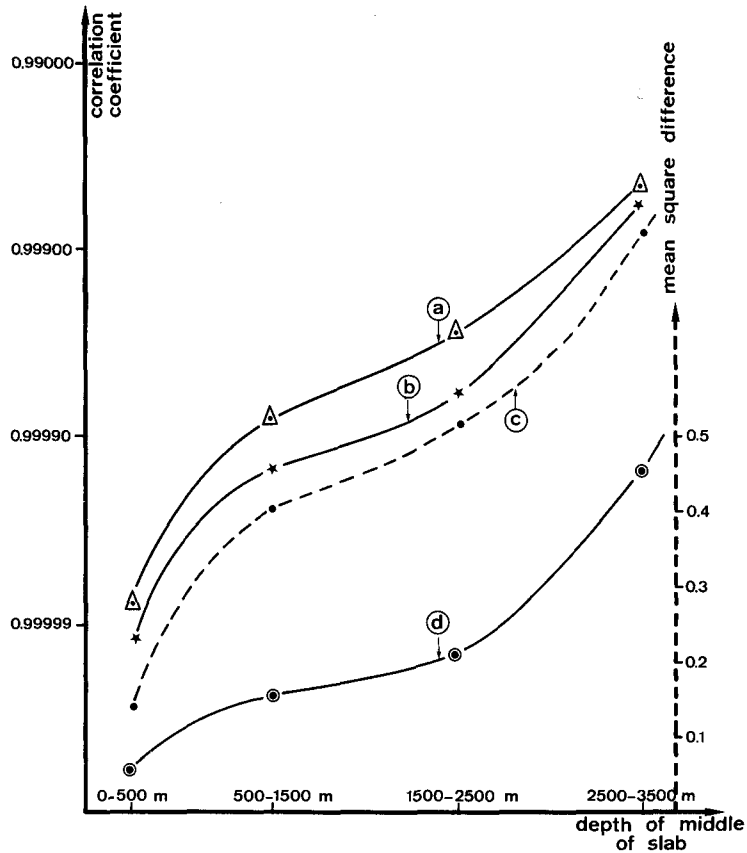

Fig. 7. Variation of mean square differences and correlation coefficients with depth. (a) Correlation coefficient, entire area; (b) correlation coefficient, main anticline; (c) correlation coefficient, southwest syncline; (d) average mean square difference. The arrow indicates average depth computed in next step.

[Variation des écarts types et des coefficients de corrélation avec la profondeur. (a) Coefficient de corrélation, ensemble de la prospection; (b) coefficient de corrélation, anticlinal principal; (c) coefficient de corrélation, synclinal du Sud-Ouest; (d) écart type moyen. La flèche indique la profondeur calculée à l'étape suivante.]

The general shape of those curves suggests that, in addition to the main causes situated at 1000–2000 m, there exists some gravimetric noise, due to superficial causes, or due to imperfections in the system itself.

These two parameters can thus be used to determine the maximum depth of gravity anomalies, similar to the rules given by Bott and Smith (1958) for simple bodies.

A third criterion is the absolute value of density variations shown in fig. 8 for the entire area, the main anticline and the southwest syncline. The values are close to the theoretical density limit (σ_0) for the outcropping slab (0–500 m), which is

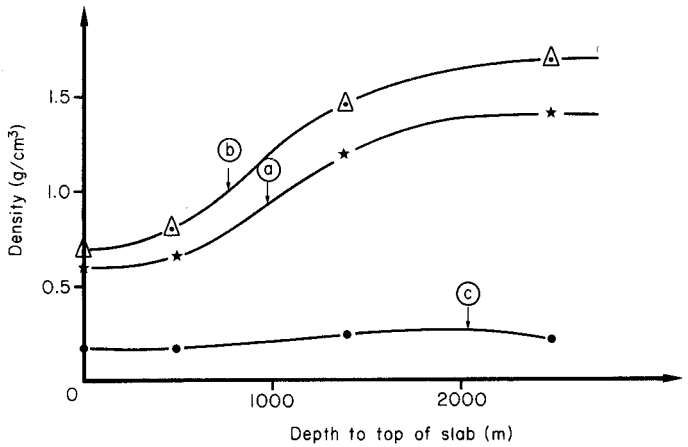

Fig. 8. Variation of densities with depth. (a) Entire area; (b) main anticline; (c) southwest syncline. The arrow indicates depth to top of slab computed in next step.

[Variation des densités avec la profondeur. (a) Ensemble de la prospection; (b) anticlinal principal; (c) synclinal Sud-Ouest. La flèche indique la profondeur jusqu'au toit de la plaque, calculée à l'étape suivante.]

$$\sigma_0 = \frac{23.87\ \Delta g_{\max}}{e}.$$

For $\Delta g_{\max} = 28.6$ mGal and $e = 500$ m, one has $\sigma_0 = 1.365$ g/cm^3 instead of the computed value of 1.4 g/cm^3. Maximum density contrast increases for depths greater than 500–700 m, considering either the whole area or the main anticline, reaching 1.4 or 1.6 g/cm^3 for depths to the top of basements of about 2000 m. These values are geologically impossible; to reduce them, it would be necessary to assume a thicker plate, bringing back the top of the plate to depths of around 1000 m (thickening the plate downwards would not substantially reduce the density contrast). The maximum density contrast thus provides another constraint on the depth to the top of the anomalous layer.

4. Structural Interpretation with Geological Constraints

In order to use a three-layer model, it was necessary to simplify the complex geology. The general stratigraphy of the area is, very schematically, as shown in table 2 (with depths relative to a datum plane 100 m above sea level).

The interpretation starts by supposing that the anomaly is due to density variations of a horizontal slab. We selected 1100 m as depth to roof and 2500 m as depth to base, following the results of the systematic interpretation by slabs and the geological data.

Table 2. *General stratigraphy of the area.*

	Presumed density (g/cm^3)	SW of the anticline	Anticline	NE of the anticline
Tertiary (sand, clay, limestone)	2.0	100 m	0	150 m
Cretaceous (chalk, mail)	2.0	100 + 150 = 250 m	0	150 + 150 = 300 m
Jurassic (marl, limestone)	2.4	250 + 1250 = 1500 m	100 m	300 + 1200 = 1500 m
Permo-Triassic (clay, sandstone)	2.4	1500 + 1000 = 2500 m	Absent	Absent
Primary (limestone, slate, sandstone)	2.4	1500 + 1000 = 2500 m	Absent	Absent
Crystalline basement (gneiss + local basalt intrusions)	2.8			

The map obtained (fig. 9) shows variations of density between -0.60 and $+0.20$ g/cm^3, that is a maximum contrast of 0.80. This excessive contrast (compared to the theoretical 2.8–2.4 = 0.4) could mean that:

—the plate is thicker than 1400 m;
—and/or more superficial anomalies are superimposed.

A first test with the same top and a higher base (in that case, Primary and Permo-Triassic sediments were included in the basement) gave even more unrealistic density contrasts. We therefore concluded that a more correct model consisted in grouping the Primary and the Permo-Triassic with the Jurassic.

Structural analysis of this density map shows many interesting features. Several secondary anticlines and synclines parallel to the main anticline can be seen. In addition, several transverse faults (NE–SW or ENE–WSW) can be seen, and should be compared to geological features described by, e.g., Weber (1973), Pomerol (1980) and Debeglia (1977).

The second step, which follows automatically, transforms these density variations into thickness changes, assuming:

—a flat base at a depth of 2500 m;
—a variable top, situated between two "buffers": the lower "buffer" at a depth of 2500 m, the upper "buffer" determined from the general geological structure, translated 100 m upwards, to allow some freedom;

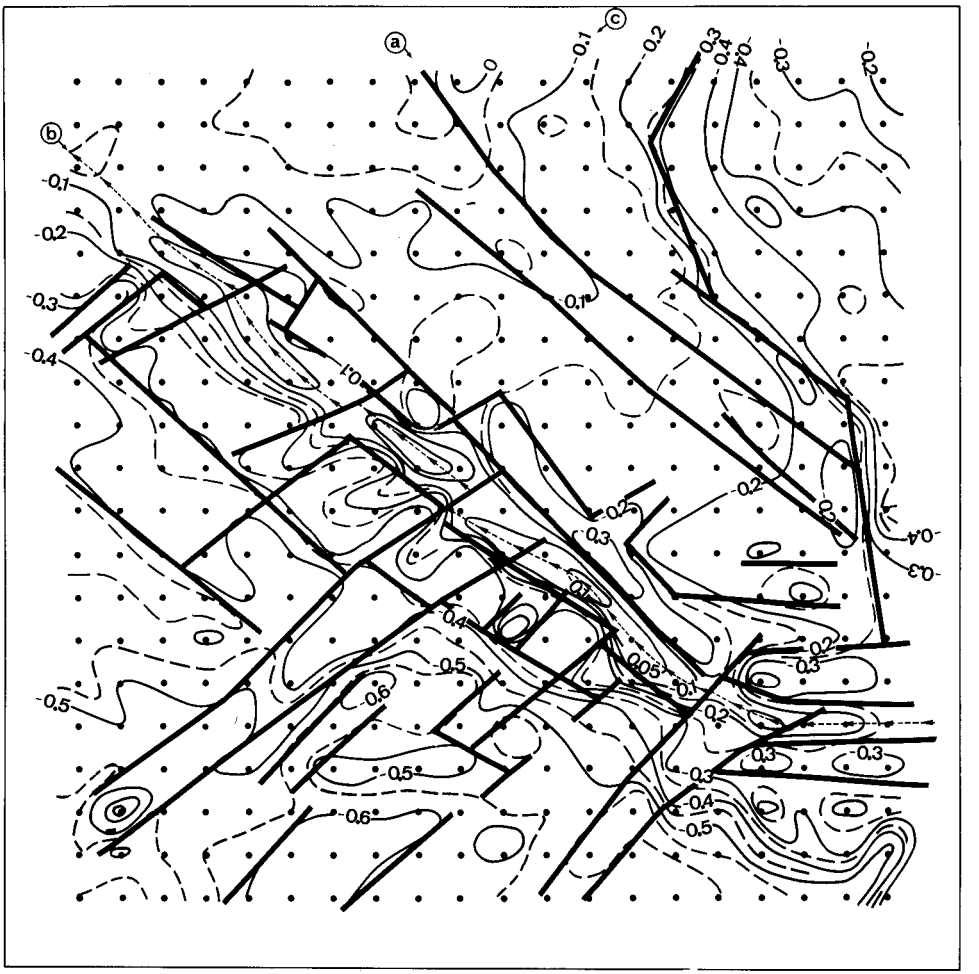

Fig. 9. Structural map, densities between 1100 and 2500 m. (a) Fault; (b) major anticline; (c) density (g/cm^3).

[Carte structurale, densités entre 1100 et 2500 m. (a) Faille; (b) anticlinal principal; (c) densité (g/cm^3).]

—a constant density contrast of 0.4 g/cm^3 (basement 2.8 g/cm^3, sedimentary strata 2.4 g/cm^3).

The upper buffer is shown on fig. 10. The transformation in each 2 × 2 km prism of densities into thicknesses is done in two steps:

—first, a linear transformation of density contrasts $\Delta\sigma$ into

$$h \approx \frac{(2500 - 1100) \times \Delta\sigma}{(2.8 - 2.4)}.$$

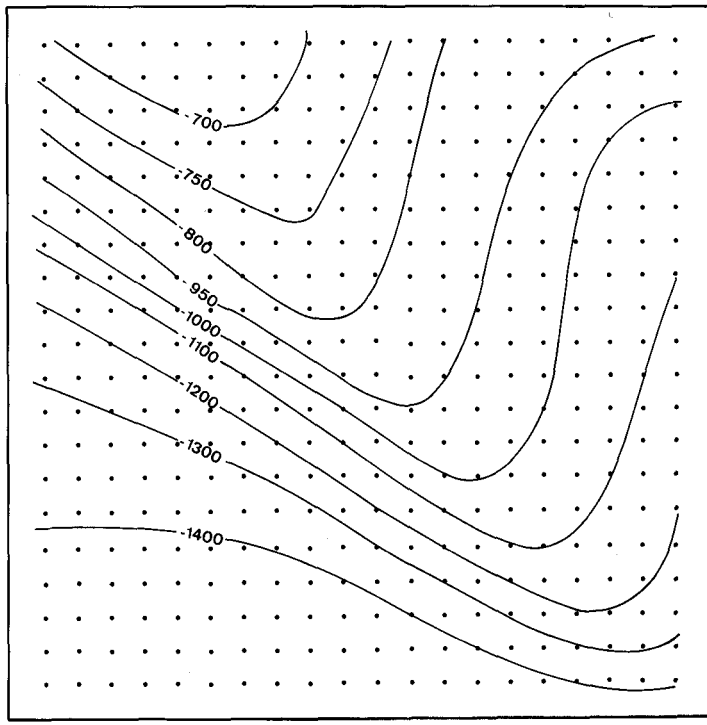

Fig. 10. Geological "buffer": minimum depths below sea level of interface between second and third layer. ["Butoir" géologique: profondeurs minimales sous le niveau de la mer, du contact entre seconde et troisième couches.]

The exact correction takes into account displacement of the prism's center of gravity and is not described here;

—a second iteration slightly modifies the top of the prism by treating differences between measured field and the field due to the approximate structure. Improvements by further iterations are very small.

After computing the final basement map, the corresponding field is computed and compared to the measured field.

The residual is mainly due to the fact that along the main anticline as well as in the northeast of the area, the buffer has often been reached. This residual is then supposed to be due to variations of a first layer located between depths of 5 and 500 m, corresponding approximately to the Tertiary and the Cretaceous (in other surveys, the residual could also have been attributed to basement density changes).

Structural analysis of this first layer is then carried out in a similar manner:

—density map between 5 and 500 m;

—transformation into changes of thickness, supposing a density contrast of 0.4 g/cm^3 (first layer 2.0 g/cm^3, second layer 2.4 g/cm^3).

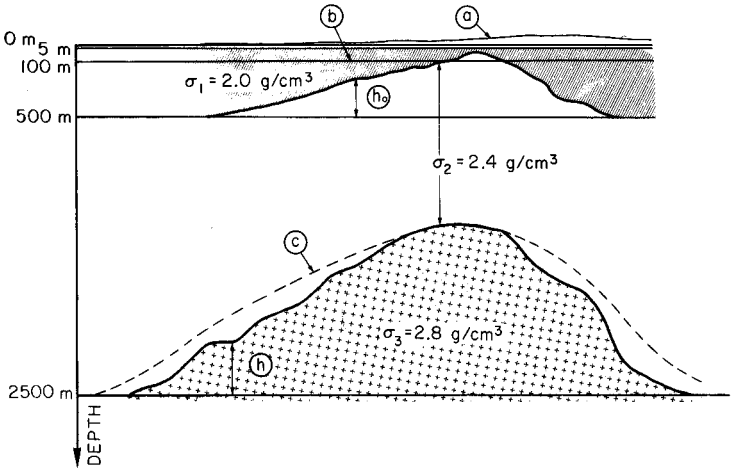

Fig. 11. Geological constraints of the model. (a) Ground level (average elevation 100 m above sea level); (b) sea level; (c) geological "buffer" for top of third layer; (h) height of interface between second and third layer limit above base (2500 m below datum); (ho) height of interface between first and second layer limit above base (500 m below datum).

[Contraintes géologiques du modèle. (a) Altitude moyenne du terrain + 100 NGF; (b) niveau de la mer; (c) "butoir" géologique pour le toit de la troisième couche; (h) hauteur de la limite 2ème–3ème couches, au-dessous d'une base située à 2500 m de profondeur; (ho) hauteur de la limite 1ère–2ème couche avec base située à 500 m de profondeur.]

A three-layer model is thus obtained. The various parameters and buffers are shown on fig. 11.

The computer program supplies the following maps:

—Bouguer anomaly;
—top of the deep structure;
—field due to the deep structure;
—difference between Bouguer and computed field;
—top of the superficial structure;
—field due to the superficial structure;
—last residual;
—for each step, difference maps and correlation maps.

The first two maps are shown in figs. 11 and 12. A general SW–NE cross-section (fig. 13) illustrates the complete interpretation.

5. Comments and Interpretation

5.1. Basement Map (fig. 12)

This map shows a series of NW–SE anticlines and synclines, parallel to the main Pays de Bray anticline. Several short transverse faults can be seen; several of them

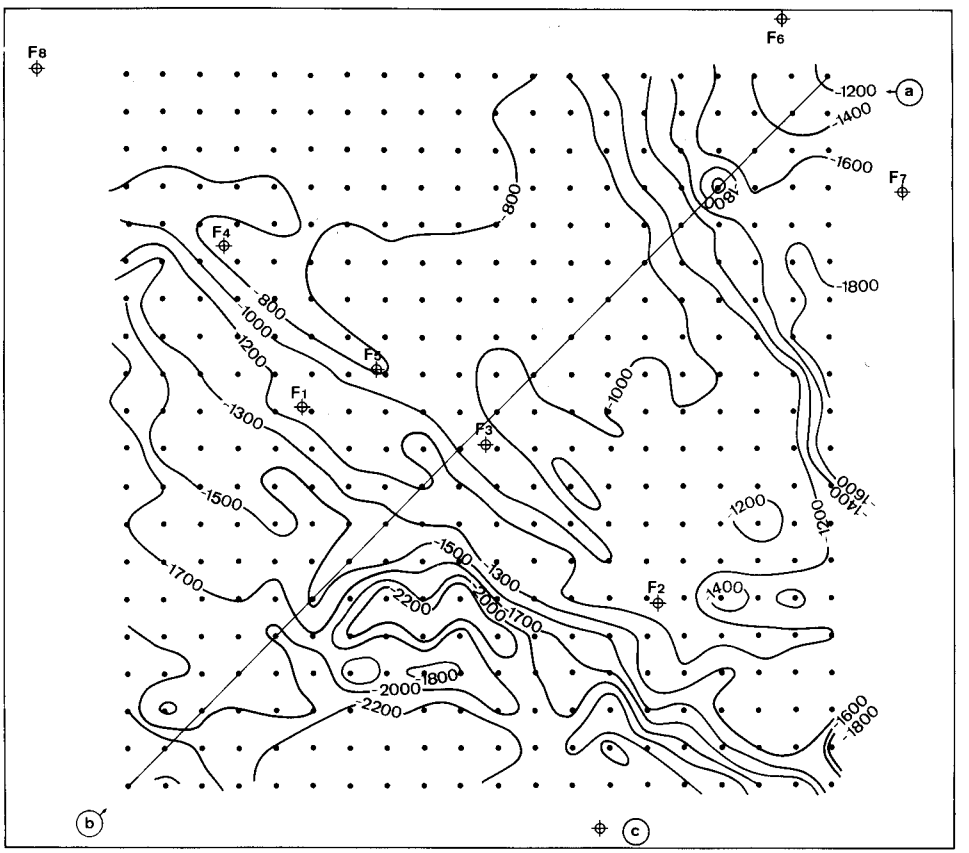

Fig. 12. Basement map. (a) Depth below sea level; (b) cross-section; (c) wells.
[Carte en courbes de niveau du socle. (a) Profondeurs sous le niveau de la mer; (b) coupe d'interprétation; (c) forages.]

seem to be connected. The main transverse fault is NE–SW and connects the center of the survey to the SW corner.

Five wells where the igneous basement was reached were compared to the final interpretation as shown in table 3.

These very small differences are surprising, particularly since well 1 is located on a secondary anticline on the southwest flank of the main anticline. This secondary anticline is practically invisible on the Bouguer map. Three other wells lie outside the survey area, two near the NE corner, and another one near the NW corner. The differences are more important:

F6 (Belleuse), real depth 871 m instead of about 1300 m;
F7 (Mardivilliers), real depth 144 m instead of about 1650 m;
F8 (Compainville, PB 201), real depth 861 m instead of about 700 m.

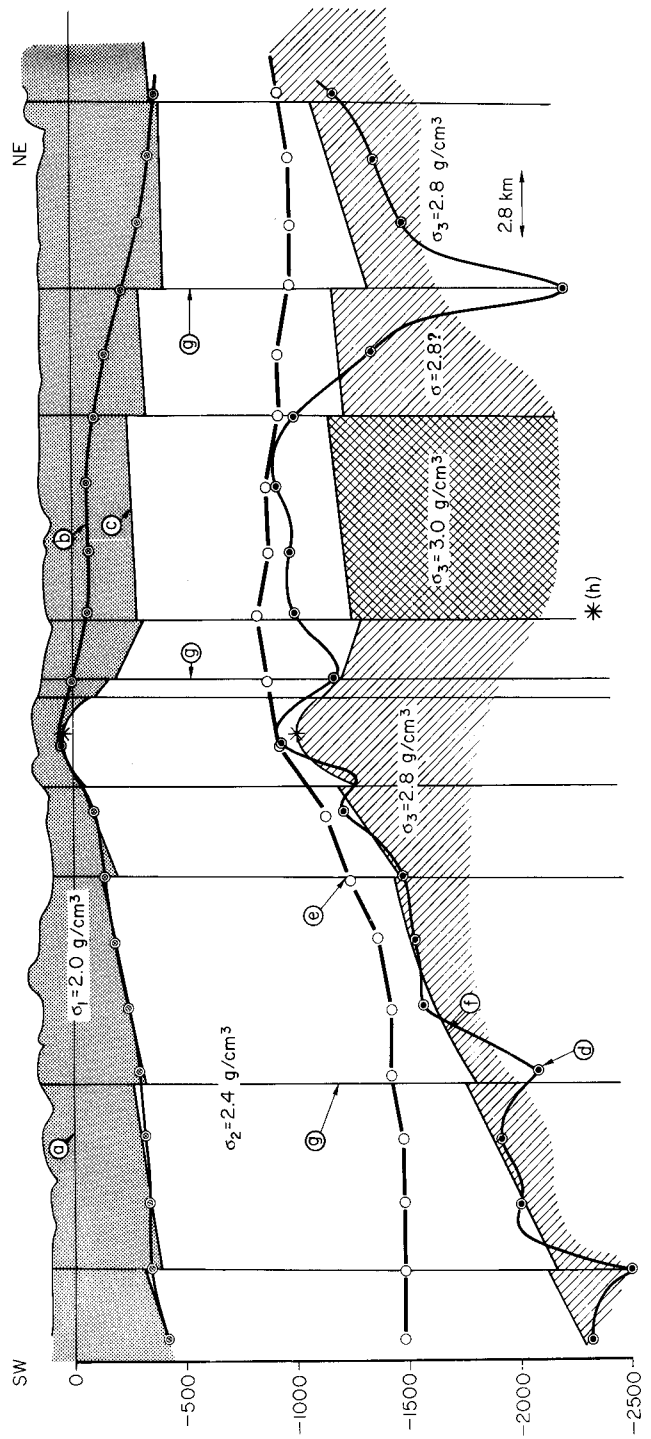

Fig. 13. Interpreted cross-section. (a) Sea level; (b) first and second layer gravity limit; (c) interpreted base of Kimmeridgien; (d) second and third layer gravity limit; (e) geological upper "buffer" for limit (d); (f) interpreted basement; (g) low density faulted zones; (h) geological boundaries, after drill holes.

[Coupe d'interprétation. (a) Niveau de la mer; (b) limite 1ère–2ème couches d'après déconvolution; (c) base interprétée du Kimmeridgien; (d) limite 2ème–3ème couches, d'après déconvolution; (e) "butoir" supérieur géologique pour la limite (d); (f) toit interprété du socle; (g) zones faillées, à plus faible densité; (h) limites géologiques, d'après forages.]

Table 3. *Comparison of depths at five wells.*

	Actual depth (m)	Computed depth (m)
Well F1 (Ferrières-en-Bray)	−1010	−1100
Well F2 (aux Marais)	−1107	−1060
Well F3 (Hodenc-en-Bray PB402)	−978	−900
Well F4 (Villers Vermont)	−859	−800
Well 5 (Hanaches PB101)	−879	−900

These differences can be explained by:

—unreliability of the extrapolation of our results out of the survey area;
—lower quality of deconvolution due to edge effects, particularly in the corners;
—for wells F6 and F7, influence of the low-density NW–SE axis crossing the NE corner of the survey;
—influence of a regional anomaly.

This last reason seems to be the most important: all the wells along the main anticline (except F1) have real depths greater than computed depths, while wells F6 and F7, near the NE corner, have real depths smaller than computed depths.

5.2. First computed field and first residual

The computed fields look very much like the Bouguer anomaly, and the residual map is more important. The mean square residual is 1.86 mGal (8.2% of the median Bouguer anomaly). The main differences are due to points where the structure reaches the buffer, principally along the main anticline. The residual map is therefore a "ghost" of the Bouguer anomaly.

5.3. Superficial structural map

The main anticline shows up clearly, as well as another parallel anticline 11 km to the NE. Three transverse features appear, one of which corresponds to the major transverse fault visible on the basement map. The northern feature was not visible on the other maps.

5.4. Second computed field and last residual

The second computed field is very similar to the first residual field. The mean square difference is 0.17 mGal, 3.8% of the average amplitude of the first residual

(4.5 mGal) or only 0.8% of the average amplitude of the original Bouguer anomaly (22.7 mGal). The figure of 0.8% is to be compared with the mean square difference of 8.2% on the basement map.

It should be noted that the remaining differences are due to:

—four points reaching the second buffer, along the main anticline, with differences of 0.63, 0.96, 0.31, and 0.37 mGal, respectively;
—edge effects.

If these four points and one line close to the margin were removed, the mean square difference would be only of 0.13 mGal (0.6%).

Taking into account these remarks, it can be seen that the last residual map still has an organized look. First, an extensive "anticline" of small amplitude, with the same axis as the main anticline, can be seen; it may be related to regional variations in the basement. This "regional" anomaly has the following values:

Northeast	−0.4 mGal;
Anticlinal axis	+0.2 to +0.3 mGal;
Southwest	−0.2 mGal.

The corresponding gradients are very small: 0.02 mGal/km.

Apart from this regional effect, two other slight "anticlines" can be seen parallel to the main anticline. However, after comparison with the basement map, it seems that the deep deconvolution was slightly too powerful and that the two synclines separated by the main anticline on the basement map are somewhat shallower than indicated. Of course, other geological interpretations are also possible.

5.5. Edge effects

The above-mentioned edge effects are mainly due to the calculation of the resultant field and not to the deconvolution itself. When this job was carried out, the resultant field was computed without extrapolation of the structure out of the survey area. Since then, the program has been adjusted to suppress this minor defect.

5.6. Final geological interpretation

The general geological interpretation is shown in fig. 13, which is a SW–NE diagonal cross-section. We have drawn:

—the interface between the second and the third layer according to deep deconvolution;
—the geological buffer;
—top of the basement (third layer);
—the interface between first and second layer according to residual deconvolution.

The comparison between the top of the second layer and our geological interpretation based on surface data shows a remarkable coincidence between this

interface and the base of the Kimmeridgian, except in an area located between 2 and 13 km NE of the main anticline. In order to have regular variation of thicknesses, it was necessary to lower both gravimetric limits. Part of the gravity high can then only be explained by an increase in basement density, which would be around 3.0 g/cm^3. This axis would correspond to the important (but rather flat) gravity high to be seen on the Bouguer map, with an axis located at 9 km NE of the main anticline. This part of the interpretation was carried out by semi-manual calculation, using the two-dimensional prism formula.

Lastly, there remain local negative differences between geological and gravity interpretation. These negative residuals are probably due to narrow vertical faulted zones, where the second layer density could be reduced to 2.3 g/cm^3 and/or the basement density reduced to 2.6 g/cm^3.

6. Comparison Between Classical Downward Continuation and Density Maps

Though this paper does not deal with the theoretical aspects of the described method, it seems useful to place what we call "deconvolution" within the context of classical map filtering by Fourier transforms or grid operators.

First, it should be noted that "gravity deconvolution" (Bichara and Lakshmanan 1979) is no more than a particular map filtering. Nevertheless, two differences between "deconvolution" and classical map filtering should be stressed:

a. Map filtering aims at obtaining either an enhancement of certain anomalies (e.g., second derivative at various grid spacing, regional or residual filtering) or a map representation of fields at different altitudes (upward or downward continuation). "Deconvolution" aims at obtaining a density distribution for a plate of chosen thickness and depth.
b. Map filtering can, at least theoretically, be done perfectly. This is due to the fact that frequency domain representations of upward, downward, and second derivative operators have analytical expressions (Fuller 1967). We do not know of any frequency domain analytical expression for density operators.

Nevertheless, one could argue that classical downward continuation is a density operator which also has the advantage of being well defined in the frequency domain, and thus would be more advantageous to use as an operator. In fact, downward continuation can only give a surface density distribution which has less physical significance and is more difficult to use for structural mapping. Another disadvantage of downward continuation is that, in our experience, it is a much more noise-generating filter than "deconvolution". In any case, downward continuation can be (and has been) used for structural mapping (La Porte 1963); in this respect, "deconvolution" could be described as a generalization of downward continuation: downward continuation is a "deconvolution" with a layer of thickness 0 and at a depth which is a multiple of the grid dimension.

7. Conclusions

The three-dimensional, three-layer deconvolution of existing gravity data along the Pays de Bray anticline has supplied a powerful structural tool to the geologists, helping to locate various features, such as secondary anticlines and transverse faults, particularly for a secondary anticline on the flank of the main one, practically invisible on the Bouguer map.

Three-layer modeling was possible here by the use of geological constraints, available in this well-known area.

The basement map compared to five wells shows a mean square difference of 72 m (6.4%). This accuracy is in part due to the absence of lateral density variations and also to an abrupt variation between sedimentary and basement densities.

In regions where no geological information is available, the described procedure results in several parameters (mean square difference, correlation coefficient, and limiting densities) that can be employed to automatically construct a maximum-depth basement map. It should be stated that the interpretation tool described in the present paper has been used regularly by us for several years; various improvements update the technique each year. Of course, this new methodology of the interpretation of gravity anomalies does not render obsolete classical interpretation methods, such as downward continuation. There will always be the necessity of separating regional trends from residual; classical methods for depth determination are always useful and we do use them frequently. Nevertheless, density maps allow a quantitative look at Bouguer anomalies which have proved useful in many instances. Furthermore, provided a given density contrast, these maps are easily transformed into basement maps, which in many cases were confirmed by drilling. We are presently studying the application of these techniques to air, land, or sea magnetic surveys.

References

Bichara, M. and Lakshmanan, J. 1979, Automatic deconvolution of gravimetric anomalies, Geophysical Prospecting 27, 798–807.

Bott, M.H.P. and Smith, R.A. 1958, The estimation of limiting depth of gravitating bodies, Geophysical Prospecting 6, 1–10.

Debeglia, N. 1977, Apports de synthèses géophysiques à la connaissance du socle du Bassin de Paris, 1977, BRGM Orléans, 77 SGN 535 GPH.

Fuller, B. 1967, Mining Geophysics, Vol. 2, published by SEG, Tulsa, October 1967.

Lakshmanan, J. 1973, Gravity and gamma-gamma mapping of sink-hole areas in Lutetian Gypsum, North East of Paris, IAEG Symposium on Engineering Geology, Hannover, September 1973.

La Porte, M. 1963, Calcul de la forme d'une structure homogène à partir de son champ gravimétrique, Geophysical Prospecting 11, 276–291.

Naudy, H. 1971, Automatic determination of depth on aeromagnetic profiles, Geophysics 36, 717–722.

Pomerol, B. 1980, Style tectonique des Pays au Nord-Ouest de l'Oise—Rôle des différentes directions structurales, Bulletin d'Information des Géologues du Bassin de Paris 17, 21–25.

Weber, D. 1973, Le socle antetriasique sous la partie Sud du Bassin de Paris d'après les données géophysiques, Bulletin BRGM Orléans, Sect. II 1973, 219–343.